

Three-dimensional printed metal-nested composite fuel grains with superior mechanical and combustion properties

Xin Lin, Dandan Qu, Xuedong Chen, Zezhong Wang, Jiaxiao Luo, Dongdong Meng, Guoliang Liu, Kun Zhang, Fei Li & Xilong Yu

To cite this article: Xin Lin, Dandan Qu, Xuedong Chen, Zezhong Wang, Jiaxiao Luo, Dongdong Meng, Guoliang Liu, Kun Zhang, Fei Li & Xilong Yu (2022) Three-dimensional printed metal-nested composite fuel grains with superior mechanical and combustion properties, *Virtual and Physical Prototyping*, 17:3, 437-450, DOI: [10.1080/17452759.2022.2035934](https://doi.org/10.1080/17452759.2022.2035934)

To link to this article: <https://doi.org/10.1080/17452759.2022.2035934>



© 2022 The Author(s). Published by Informa UK Limited, trading as Taylor & Francis Group



Published online: 18 Feb 2022.



Submit your article to this journal [↗](#)



Article views: 1661



View related articles [↗](#)





View Crossmark data [↗](#)



Citing articles: 3 View citing articles [↗](#)

Three-dimensional printed metal-nested composite fuel grains with superior mechanical and combustion properties

Xin Lin ^{a,c}, Dandan Qu ^b, Xuedong Chen^d, Zezhong Wang^a, Jiaxiao Luo^{a,c}, Dongdong Meng^{a,c}, Guoliang Liu^b, Kun Zhang^{b,c}, Fei Li^{a,c} and Xilong Yu^{a,c}

^aState Key Laboratory of High Temperature Gas Dynamics, Institute of Mechanics, Chinese Academy of Sciences, Beijing, People's Republic of China; ^bWide Range Flight Engineering Science and Application Center, Institute of Mechanics, Chinese Academy of Sciences, Beijing, People's Republic of China; ^cSchool of Engineering Science, University of Chinese Academy of Sciences, Beijing, People's Republic of China; ^dDepartment of Applied Mechanics, China Agricultural University, Beijing, People's Republic of China

ABSTRACT

The mechanical and combustion properties of metal-nested composite hybrid rocket fuel grains composed of spiral aluminium (Al) frameworks fabricated using three-dimensional (3D) printing with an embedded paraffin-based fuel were investigated. The mechanical properties of the resulting grains were evaluated by compression tests. In addition, the combustion characteristics of the Al composite grains were examined in a lab-scale hybrid rocket engine with gaseous oxygen as the oxidizer at an initial mass flow rate of 17.9 g/s. Pure paraffin-based (PP) and acrylonitrile-butadiene-styrene (ABS) composite grains were also tested as baseline fuels for comparison. The Al-A composite grain exhibited superior mechanical and combustion properties, with Young modulus, yield stress, and regression rate increased by 757.1%, 381.3% and 52.5% compared with the PP grain. The Young modulus and combustion efficiency were also further improved, by 51.0% and 14.9%, respectively, by including perforations in the spiral blades. These improvements are discussed in detail herein based on experimental data together with numerical simulations. Emission spectra of the engine plumes were also acquired and used to qualitatively analyze the combustion characteristics of the Al blades.

ARTICLE HISTORY

Received 12 December 2021
Accepted 27 January 2022

KEYWORDS





Hybrid rocket engine; additive manufacturing; metal-nested composite fuel grain; mechanical properties; combustion properties; optical emission spectroscopy

Introduction

Hybrid rocket engines (HREs) combine the intrinsic advantages of liquid propellants and solid fuels, which renders it simple structure, high safety and reliability, adjustable thrust, and lower cost than conventional rocket engines (Whitmore, Sobbi, and Walker 2014; Wang et al. 2021a; Cai et al. 2013; Fang et al. 2021; Zilliac et al. 2020; Kahraman, Ozkol, and Karabeyoglu 2021). These advantages make HREs attractive with regard to a broad range of space applications, such as sounding rockets (Sella et al. 2020; Bouziane et al. 2019; Broughton et al. 2018; Marciniak et al. 2018), upper stage propulsion units (Jens, Cantwell, and Hubbard 2016; Casalino and Pastrone 2008) and commercial manned spacecrafts (Cai et al. 2013; Mazzetti, Merotto, and Pinarello 2016). However, HREs have several associated challenges, the most significant being the low regression rates of classical polymeric

fuels. The issue of low regression rates has thus far seriously restricted the implementation of HRE technology in large-scale thrust applications (Kobald et al. 2017).

The structural and chemical modifications of fuel grains are the main strategies that have been suggested to date to mitigate this drawback. These modifications have included the use of multiple ports to increase the surface area of the grain, complex port geometries to increase turbulence in the combustion chamber, certain energetic additives to strengthen heat transfer and the development of liquefying fuels, such as paraffin waxes (Kuo and Chiaverini 2007; Tian et al. 2017; Shinohara and Nakagawa 2012; De Luca et al. 2017; Karabeyoglu, Altman, and Cantwell 2002; Akhter and Hassan 2018; Zhang, Hu, and Zhang 2016; Whitmore et al. 2015; Karabeyoglu and Altman 1999; Veale et al. 2018). All of these techniques have demonstrated some ability to increase regression rates but have also introduced many other issues. As an example, the

CONTACT Dandan Qu  dandanqu@imech.ac.cn  Wide Range Flight Engineering Science and Application Center, Institute of Mechanics, Chinese Academy of Sciences, No.15 Beisihuanxi Road, Beijing 100190, People's Republic of China; Zezhong Wang  wangzezhong@imech.ac.cn  State Key Laboratory of High Temperature Gas Dynamics, Institute of Mechanics, Chinese Academy of Sciences, No.15 Beisihuanxi Road, Beijing 100190, People's Republic of China

© 2022 The Author(s). Published by Informa UK Limited, trading as Taylor & Francis Group
This is an Open Access article distributed under the terms of the Creative Commons Attribution-NonCommercial-NoDerivatives License (<http://creativecommons.org/licenses/by-nc-nd/4.0/>), which permits non-commercial re-use, distribution, and reproduction in any medium, provided the original work is properly cited, and is not altered, transformed, or built upon in any way.

multiple port approach decreases the volume utilization efficiency in the engine, increases the manufacturing difficulty and cost, and increases the risk of structure collapse of the grain and feed-coupled instabilities between the injectors and the multiple fuel ports (Kuo and Chiaverini 2007). In addition, the regression rate enhancement obtained using the complex port geometries is reduced as the grain is consumed during the combustion processes because the characteristic structure of the fuel grain gradually recedes (Whitmore et al. 2015). The incorporation of metal particles in the fuel grain increases production costs and makes it very difficult to use traditional cast/cure techniques (De Luca et al. 2017; Whitmore et al. 2015). Although paraffin-based fuels tend to exhibit superior regression rates as a result of droplet entrainment, pure paraffin fuels show poor mechanical strength and require reinforcing binders or a support structure, both of which can lower the regression rate (Karabeyoglu, Altman, and Cantwell 2002).

In recent years, additive manufacturing (AM, also referred as three-dimensional (3D) printing) undergone rapid development and has been successfully used to manufacture various key components of rockets, such as injectors, igniters, combustion chambers and nozzles. There has also been significant progress in the fabrication of hybrid rocket fuel grains having enhanced regression rates (Zdybal et al. 2021; Oztan et al. 2021; Oztan and Coverstone 2021; Ozawa et al. 2020; Hill et al. 2019; Hitt 2018; Bisin et al. 2020a; 2020b; Whitmore and Walker 2017; Joshi and Sheikh 2015; Whitmore, Peterson, and Eilers 2013; Wang et al. 2020, 2021b; Pabarcus 2019; Arnold et al. 2013; Connell et al. 2019; Arnold et al. 2014; Young et al. 2021; Whitmore et al. 2021). AM enables polymeric fuel grains having complex geometries, such as helical or star-swirl ports and protruding vane turbulator centre ports, to be rapidly and easily generated. Such geometries would be difficult to form by traditional manufacturing methods. One of the most representative works in this field was published by Whitmore et al. (2015), who achieved a significant improvement in the regression rate and specific impulse of acrylonitrile-butadiene-styrene (ABS) grains by tailoring the chemical composition and manufacturing a helical port structure. Recently, Young et al. (2021) developed custom-made 3D printed filaments comprising poly (methyl methacrylate) and 0–25 wt% aluminium (Al) additives, and investigated the combustion characteristics of grains with a swirl-ellipse geometry made from these novel materials. Firing tests showed that the combination of metallic particles and a swirl-ellipse geometry resulted in an enhanced regression rate.

Another application of the AM technique that differs from fully 3D printed fuel grains is the use of printed structures as supports for pure paraffin fuel. This technique increases mechanical strength of the paraffin while maintaining its inherently high regression rate. Hill et al. (2019) used polylactic acid (PLA) to fabricate a single port framework having a custom lattice structure consisting of continuous gyroid surfaces, the voids of which were filled with a 99:1 (by mass) mixture of paraffin wax and carbon black. Firing results showed that this lattice structure effectively decreased sloughing of the paraffin and improved combustion stability, albeit at the expense of a minimal decrease in regression rate. Bisin et al. (2020a, 2020b) proposed a similar paraffin-based fuel termed an 'armored grain' that was made of pure paraffin embedded in a 3D printed cellular structure composed of ABS, poly(lactic acid) and nylon. Compression tests showed that the reinforcement provided by the gyroid structure improved the mechanical strength of the paraffin wax, with the nylon-based armored grains exhibiting the most enhancement.

Our own group previously proposed a similar strategy (Wang et al. 2020, 2021b). This prior work demonstrated a novel composite fuel grain based on two fuels with different regression rates that generated a swirl flow and enhanced turbulence, thereby improving the regression rate and combustion efficiency. This composite grain consisted of paraffin-based fuels (Wu et al. 2018) (86% by weight) embedded in a 3D printed helical ABS structure (14% by weight). Experimental results confirmed that the nested helical structure was maintained throughout the combustion process, in contrast to the behaviour of completely 3D printed fuel grains (Whitmore et al. 2015; Young et al. 2021). The regression rate of this composite fuel grain was also significantly improved compared with that of a traditional paraffin-based fuel and could be further increased by increasing the oxidant flux. However, this prior work did not involve conduct mechanical testing of the fuel grain.

The present work demonstrates a metal-nested composite hybrid rocket fuel grain fabricated via the AM of a helical Al framework followed by the casting of a paraffin-based fuel. The metal structure was designed to enhance the mechanical properties of the composite fuel grain while also improving heat transfer from the flame to the paraffin-based fuel, thereby further increasing the regression rate. The mechanical properties of this grain were investigated by compression tests and were compared with those of an ABS composite grain and a pure paraffin-based (PP) grain. The combustion behaviours of the composite grains were also experimentally investigated in laboratory-scale hybrid rocket engines.

The combustion chamber pressure, time-averaged regression rate and combustion efficiency of each grain were all assessed and are discussed in detail herein. PP grains were also examined to provide a performance baseline for comparison with the composite fuel grains. A heat transfer computational fluid dynamics (CFD) study was undertaken to analyze the effect of the metal framework on the regression rate. Finally, optical emission spectroscopy (OES) was used to probe for AIO radicals generated during combustion of these grains as a means of qualitatively characterizing the combustion of the 3D printed Al framework.

Experimental

Fuel grain fabrication

The two-step strategy used to fabricate the metal-nested composite fuel grains is illustrated in Figure 1. A fuel framework (Figure 1(a)) having multiple inner spiral blades was designed using 3D graphics software and fabricated employing the AM method. This framework was meant to provide mechanical support to the paraffin-based fuel and also served as an additional fuel. The framework comprised an outer wall and twelve integrated blades spiraling in the axial direction. The length, outer diameter and inner diameter of the fuel framework were 100, 60, and 20 mm, respectively. A molten paraffin-based fuel (held at approximately 120 °C) was transferred into this framework using a centrifugal casting process until it completely filled the voids between the blades. This paraffin-based fuel served as the primary

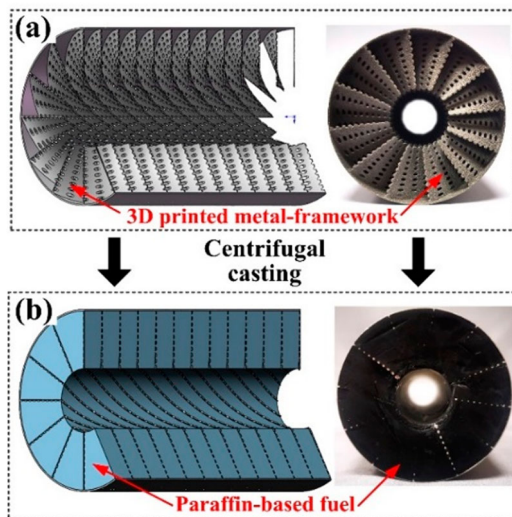


Figure 1. The two-step strategy used to fabricate the composite fuel grains. (a) The 3D printed framework with a length of 100 mm, an outer diameter of 60 mm and an inner diameter of 20 mm. (b) The nested helical structure of the composite fuel grain.

component of the composite fuel grain. The mechanical properties of this paraffin-based fuel were enhanced by incorporating multiple additives and the details of the fuel formulation and combustion performance of this material can be found in a previous paper (Wang et al. 2020, 2021b). During cooling and solidification of the paraffin-based fuel, the centrifugation rate was 1400 rpm to generate sufficient centrifugal force and multiple castings were performed to minimize thermal stress and prevent internal cracks or defects. Figure 1 (b) presents a diagram of the framework after filling with the paraffin-based fuel, showing that the metal blades maintained their initial inner diameters after casting.

Two different blade structures were used to fabricate the fuel framework, referred to herein as type A (which had no holes) and type B (which contained evenly distributed holes each with a diameter of 1 mm and a pitch of 2 mm, and a swept helically pitch of 25 mm along the grain axis), as shown in Figure 2(a–d). The perforated structure was designed to inhibit any debonding caused by material incompatibility and thus to increase the mechanical properties of the nested fuel grain. A second goal was to increase the contact area between the blades and the flame to improve the combustion efficiency of the grain.

The nested helical substrate structures were made of either Al particles or ABS and were fabricated by employing the AM process. The Al framework was supplied by the LiM Laser Technology Co. (Tianjin, China) and had a blade thickness of just 0.5 mm. The ABS framework was fabricated using a commercial 3D printer (Raise3D N2 Plus) in our laboratory. The blades of this structure were thicker (1.5 mm) to prevent thermal deformation because the deformation temperature of ABS is approximately 120 °C. Finally, a PP fuel grain was also manufactured as the baseline for comparison tests, having dimensions equivalent to those of the 3D printed fuel grains, as shown in Figure 2(e). The mass-based proportions of the nested composite fuel grains (not including the outer wall of the fuel grain) are summarized in Table 1.

Compression testing

Uniaxial compression tests were conducted on the paraffin-based fuel, 3D printed Al composite grains and 3D printed ABS composite grains using an MTS810 universal testing machine equipped with a 100 kN load cell. All tests were carried out at ambient temperature ($T = 293 \pm 5$ K) at a compression rate of 1 mm/min. One or two specimens were tested per each type. A maximum strain of 14% was applied because the

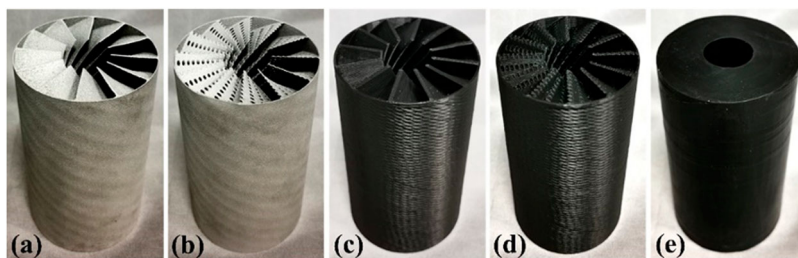


Figure 2. Photographic images of the four 3D printed frameworks and of a pure paraffin-based fuel grain. The (a) type A aluminium (Al-A) (b) type B aluminium (Al-B), (c) type A ABS (ABS-A) and (d) type B ABS (ABS-B) structures. (e) The PP-based fuel grain.

specimens showed obvious buckling above this value. Computed tomography (CT) was used to assess the grains following compression tests. The ABS composite grains were employed as model samples to investigate meso-damage, by acquiring CT images at 0.5 mm intervals along the height direction.

Lab-scale hybrid rocket engine

Figure 3 provides a diagram of the lab-scale hybrid rocket engines used in this work and further details regarding the test apparatus can be found in our previous publications (Fang et al. 2021; Wang et al. 2020). The engines employed pure gaseous oxygen as the oxidizer and a methane/oxygen torch activated by an automobile spark plug was used as the igniter. The oxidizer inlet and the igniter were positioned at the head of the engine. The oxygen flow rate was controlled by a mass flow controller (Bronkhorst, model F-203AV) and an initial mass flow rate of 17.9 g/s was used for all firing tests in this study. The length and inner diameter of the main combustion chamber were 100 and 60 mm respectively, which were consistent with the length and outer diameter of the fuel grain. The chamber pressure was monitored by two pressure transducers placed in the pre-chamber and aft-chamber, respectively. A conical nozzle was attached to the aft-chamber exit having throat and outlet diameters of 5 and 10 mm, respectively.

A spectrometer (AvaSpec-ULS2048CL-EVO, Avantes Inc.) equipped with a CMOS sensor (2048 × 1 pixel

linear array) was used to acquire emission spectra from the high-temperature plume to determine whether AIO was produced. This was done because AIO is an important intermediate product showing that Al actually participated in the combustion. The spectral resolution of the spectrometer was 0.25 nm and spectra were collected through a quartz lens having a 5 mm diameter, a focal length of 25 mm and an optical path perpendicular to the plume axis. The exposure time of the spectrometer was set to 50 ms with a repetition rate of approximately 20 Hz. The spectrometer was calibrated using a National Institute of Standards and Technology traceable quartz-tungsten-halogen standard reference lamp (Model 63945, Oriel Inc.). The spectrometer was triggered to acquire data simultaneously with engine ignition. In addition, the engine ignition, combustion and shutdown were all recorded using a Nikon single lens reflex camera.

Results and discussion

Mechanical properties

Compression tests were performed to determine and compare the mechanical properties of the five fuel grains. The resulting stress-strain curves are presented in Figure 4. Note that these data are in the form of ensemble average curves generated by averaging two tests and that the error bars indicate standard deviation. The primary results from these tests are summarized in Table 2. Each stress-strain curve exhibits an initial linear increase up to the elastic limit and yield point of the specimen. Compared with the PP grain, the ABS composite grains had higher Young modulus values (52.3% for Type A and 70.2% for Type B) and yield stresses (98%–99%). The Al composite grains exhibited ultra-high Young modulus values (757.1% for Type A and 1194.0% for Type B) and yield stresses (381.3% for Type A and 348.0% for Type B) compared with the PP composite grain. The Al substrate provided exceptional mechanical properties to the grains, which is proved by the linetype. After the yield point, the Al composite

Table 1. Mass distributions of the nested composite fuel grain without the outer wall.

Fuel grain	Total mass g	Blades of the framework		Paraffin-based fuel	
		g	wt.%	g	wt.%
Al - A composite grain	241.0	36.4	15.1%	204.6	84.9%
Al - B composite grain	234.4	28.5	12.2%	205.9	87.8%
ABS - A composite grain	204.7	37	18.0%	167.7	82.0%
ABS - B composite grain	204.9	31.9	15.6%	173.0	84.4%
PP fuel grain	234.7	0	0.0%	234.7	100.0%

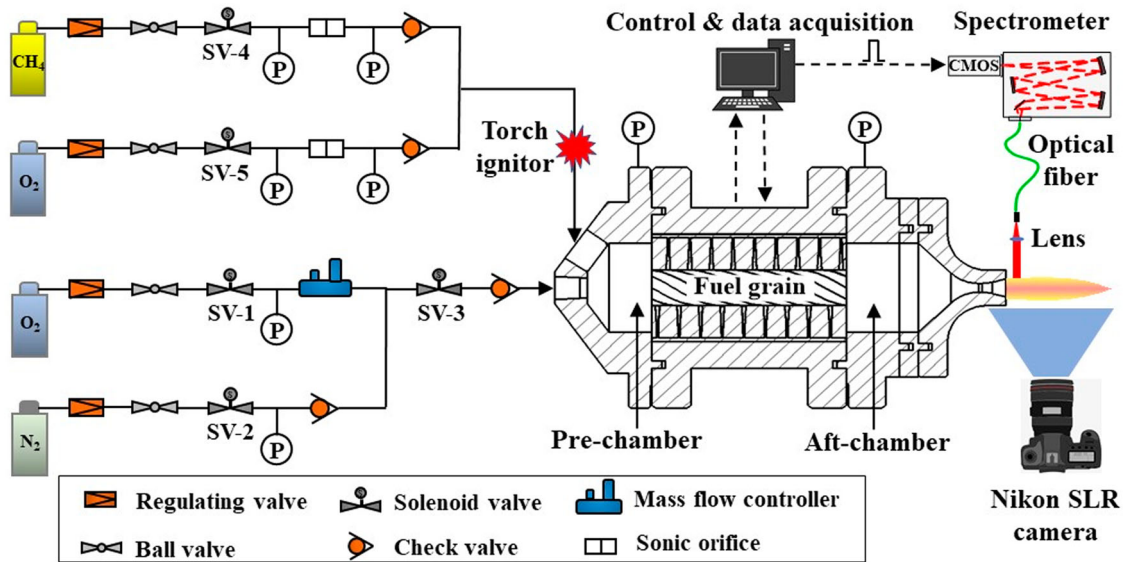


Figure 3. Schematic of the experimental setup used for the lab-scale hybrid rocket motor tests.

grains showed post-yield softening, in accordance with the stress–strain curve of an Al substrate. In contrast, the PP grain and ABS composite grain generated nearly constant post-yield stress values, as a consequence of shear deformation behaviour. Interestingly, the Young modulus of the Al-B composite grain was much higher than that of the Al-A grain, and this difference is attributed to the lattice structure formed

by the many evenly spaced holes in the latter specimen. The lattice structure of the Al-B grain was evidently able to better absorb energy and undergo elastic recovery.

The excellent mechanical properties are expected to retain at elevated temperature. Comparing to extremely low softening temperature of paraffin, softening temperature of material Al is up to 473 K (Cao et al. 2021; Uzan et al. 2018). With further increasing of temperature,

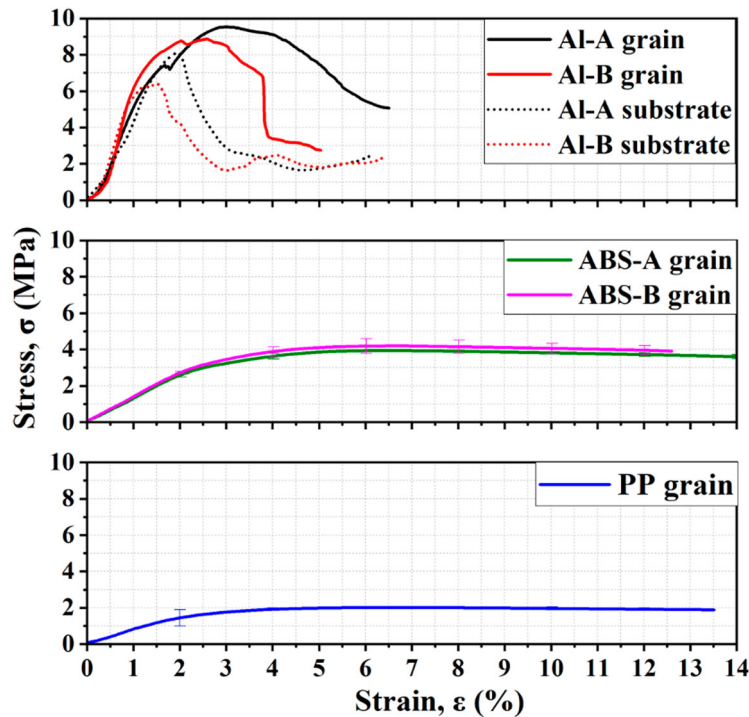


Figure 4. Stress-strain curves obtained from the nested composite fuel grains and Al substrate (all are ensemble average curves except for the Al composite grain and Al substrate, compression rate 1 mm/min, testing temperature 293 ± 5 K).

Table 2. Mechanical properties of the fuel grains determined at a compression rate of 1 mm/min and 293 ± 5 K.

Specimen	Young modulus, E [MPa]	Yield stress, σ_y [Mpa]	Yield strain, ϵ_y [%]
Al - A substrate	578 ± 11.4	8.09	2.75
Al - B substrate	844 ± 3.1	6.40	2.02
ABS - A substrate	98 ± 0.3	2.12	3.86
ABS - B substrate	95 ± 0.2	2.07	3.53
Al - A composite grain	720 ± 4.12	9.53	4.00
Al - B composite grain	1087 ± 5.2	8.87	2.70
ABS - A composite grain	128	3.93	8.67
ABS - B composite grain	143	3.95	8.36
PP grain	84 ± 0.39	1.98	7.33

AM Al begins to soften at least longer than 1800 seconds. Nevertheless, mechanical properties of AM Al are still higher than as-cast Al due to mix strengthening mechanism (Cao et al. 2021).

The photographic images in Figure 5 show that visible damage occurred in the end region of the Al composite grains without any drum-shaped deformation, while obvious drum-shaped deformation occurred during compression of the ABS and PP grains. These results are consistent with the stress-strain curves of the various specimens. These different behaviours are attributed to the stress distributions in the ABS substrate and PP grain. Regarding the Al composite grains, the Al substrate bore the majority of the stress because there was an order of magnitude difference in the mechanical properties of the Al, and the mechanical behaviour of the thin Al substrate was not the same as that of bulk Al. CT scans of the compressed ABS-A composite grain were acquired and the results showed that the maximum damage occurred in the end region (labelled D in Figure 5), as was also observed for the Al composite grain. Cracking and fragmentation of the grain as well as rupture of the substrate were apparent in the middle

region (labelled A), while regions B, C and A along the centre of symmetry of the grain all showed different extents of meso-damage. Specifically, severe deformation of the substrate and separation between the substrate and grain appeared in region B, while a lesser degree of separation between the substrate and grain was found in region C.

Combustion characteristics of the nested composite fuel grain

Variations of combustion chamber pressure

Static rocket engine firing tests were conducted with each of the composite grains and the PP grain. The data from these tests are summarized in Table 3, including the average combustion chamber pressure, P_c , burn time t_{burn} , average steady state combustion chamber pressure $P_{c,ss}$, initial oxygen mass flux G_{ini} , and average oxygen mass flux G_{ave} .

The combustion chamber pressure provides valuable information regarding the operating status of the engine, and Figure 6 presents the pressure – time histories for all firing tests. Note that each trial used the same oxidizer mass flow rate and fuel grain inner diameter. The timing sequence for the oxidizer flow initiation and shutoff and engine ignition are also included in Figure 6. Notably, the timing sequence for each test was not exactly the same, as a result of delays in the opening of valves and the execution of commands from the control system. The time axis in these plots has been offset to use time zero as the time of ignition so as to align the various pressure curves, and the burn time is defined as the time between engine ignition and oxidizer flow shutoff. After ignition at 0.0 s, a sharp increase in the combustion chamber pressure is apparent, indicating that the composite fuel grains showed similar ignition

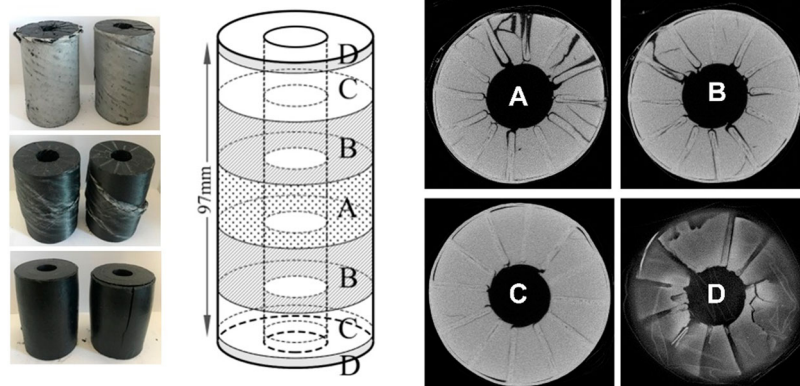
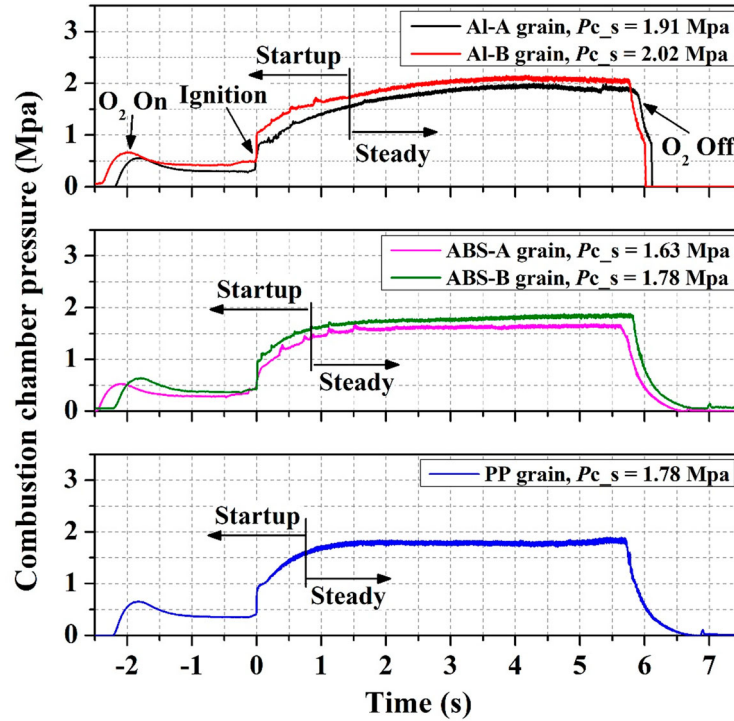
**Figure 5.** Photographic and CT images of a compressed ABS-A composite grain.

Table 3. Overall engine data for hot firings.

No.	Fuel grain	$P_{c,r}$ Mpa	t_{burnr} s	$P_{c,sr}$ Mpa	G_{inir} g/(mm ² ·s)	G_{aver} g/(mm ² ·s)
1	Al – A composite grain	1.72	5.91	1.91	5.8	3.2
2	Al – B composite grain	1.87	5.78	2.02	5.7	3.3
3	ABS – A composite grain	1.56	5.71	1.63	6.1	3.8
4	ABS – B composite grain	1.71	5.83	1.78	5.6	3.6
5	PP grain	1.73	5.73	1.78	5.6	3.8
	$e_{measure}$	±1.0%	±1.4%	±1.0%	±1.2%	±1.2%


Figure 6. Pressure vs. time histories for all firing tests performed under identical experimental conditions.

characteristics to the PP fuel grain. The combustion of these specimens can be divided into two major stages: startup and steady state. The startup period comprised the ignition process and a stepwise increase in combustion pressure to approximately 85% of the maximum value. At this point, the engine was considered to have achieved a steady state until the oxidizer flow was shut off and the average pressure during this stage was characterized $P_{c,s}$.

Figure 6 shows some discrepancies in the startup and steady state characteristics of the composite grains compared with the PP grain. Specifically, the composite grains (especially the Al grains) took longer to stabilize than the PP grain. Another discrepancy is that the $P_{c,s}$ values of the Al composite grains were obviously higher than those of the other two types of samples. These variations between samples are ascribed to increased regression rates in the Al grains. Following engine ignition, more time would be required for the

fuel mass flow rates of grains having higher regression rates (such as the Al composite grains) to stabilize, resulting in longer startup stages. Prior to steady state combustion, the regression rate would also be further increased as a result of the synergistic effect of the nested helical structure on the inner surface of the fuel grain and the high thermal conductivity of the Al blades, such that $P_{c,s}$ was increased. In addition, the participation of Al in the combustion process further increased the flame temperature, which also partially explains the increase in pressure.

Regression rate

The fuel regression rate is one of the most critical parameters associated with hybrid rocket engines. The average regression rate \dot{r}_{ave} can be calculated as

$$\dot{r}_{ave} = \frac{d_f - d_0}{2t_{burn}} \quad (1)$$

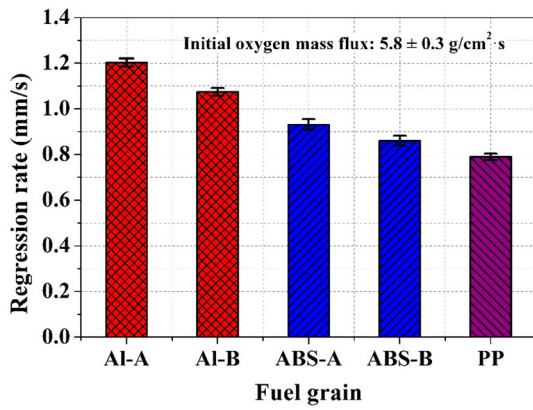


Figure 7. Comparison of regression rates of the Al composite fuel grains, ABS composite fuel grains and PP fuel grain.

where d_0 and d_f represent the average inner diameters of the fuel grain before and after the firing test, respectively. Here, the d_f is calculated as

$$d_f = \sqrt{d_0^2 + \frac{4(m_{f0} - m_f)}{\pi\rho L}} \quad (2)$$

where m_{f0} and m_f are the mass of the fuel grain before and after the firing test, L is the length of the cylindrical fuel grain, and ρ is the average density of the fuel grain. This latter term is equal to

$$\rho = \rho_p\omega_p + \rho_{3D}\omega_{3D} \quad (3)$$

where ρ_p and ω_p are the density and mass fraction of the nested paraffin-based fuel, respectively, and ρ_{3D} and ω_{3D} represent the density and mass fraction of the 3D printed material, respectively. Further details related to determining the regression rates of the nested composite fuel grains can be found in our previous work (Wang et al. 2020).

Figure 7 summarizes the regression rate of each fuel grain when using the same initial oxidizer mass flux and demonstrates that the regression rates of the composite grains were higher than that of the PP grain. Compared with the PP grain, the regression rates of the ABS-A and ABS-B grains were increased by 18.0% and 9.0%, respectively. These results confirm the positive effect of the

nested helical structure with regard to improving the regression rate, as a consequence of the difference in the regression rates of the 3D printed blades and the paraffin-based fuel. A discussion of the regression rate improvement mechanism is provided in a prior publication by our group (Wang et al. 2020). Surprisingly, the regression rates of the Al-A and Al-B grains were increased by 52.5% and 36.1% compared with the PP grain, respectively. This result demonstrates that the use of metal blades further increased the regression rate of the nested helical structure. The primary reason for this improvement is believed to be the enhanced heat transfer from the flame to the PP fuel via the metal blades. Notably, the regression rates of the grains having perforated structures were lower than those of the non-perforated structures. This discrepancy is discussed in detail in Section C in conjunction with an analysis of the heat transfer characteristics of the blades based on CFD simulations.

Thermal analysis of the swirl blade interface

Computational heat transfer simulations were used to assess the effect of the heat transfer characteristics of the spiral blades on the regression rate of the composite fuel. To facilitate these simulations, the combustion was modelled in a simplified manner using a high temperature thermal boundary for the heat transfer process. In addition, a uniform thermal boundary condition was applied along the axial direction of the grain, assuming that heat transfer only took place in the radial direction. A typical computational domain is shown in Figure 8, representing the internal volume of the combustion chamber, the 3D printed framework and the PP fuel. The thermal properties of the Al, ABS and paraffin employed in these calculations are summarized in Table 4.

The heat transfer simulations were performed using the ANSYS Fluent software in conjunction with a model containing 330,000 structural cells to discretize the computational domain. The inner and outside boundaries were modelled with high temperature (3000 K) and low temperature (300 K) conditions, respectively, while the top and bottom sides of the computational domain were assigned adiabatic conditions. A total of 5000 iterations was used for each individual

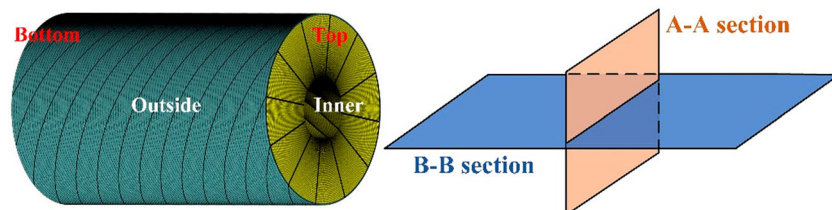


Figure 8. A typical computational mesh used to model the fuel grain during simulations.

Table 4. Thermal properties of the fuels.

Fuel	Density, ρ [kg/m ³]	Isotropic thermal conductivity λ_s [W/(m·K)]	Specific heat c_f [J/(kg·K)]
Al	2719	202.4	871
ABS	1030	0.1997	1400
Paraffin	920	0.45	2100

simulation to ensure convergence of the temperature distribution.

Figure 9 shows the calculated temperature contours for all the fuel grains in the A-A and B-B sections. It is evident that there were no significant differences in the temperature distributions of the ABS composite grain and PP grain as a consequence of the similar thermal conductivities of ABS and paraffin. However, regarding the Al composite grains, distinct star-shaped and zigzag-like temperature distributions can be observed in the A-A and B-B sections, respectively. These results can be attributed to the higher thermal conductivity of Al (approximately three orders of magnitude greater than that of ABS), which promoted heat transfer from the high temperature inner zone to the interior of the PP fuel. The superior thermal conductivity of the Al blades therefore increased the pyrolysis rate of the adjacent PP and accelerated the formation of the nested helical structure in the composite grain. These phenomena all contributed to the increased regression rates of the Al composite grains. The data also show that the star-shaped and zigzag-like area of the Al-B specimen was slightly smaller than that of the Al-A sample. The holes patterned into the blade evidently hindered heat transfer and reduced the swirling flow induced by the helical structure, resulting in a lower regression rate in the case of the perforated structure.

Combustion efficiency

Combustion efficiency is another important parameter by which the performance of an engine can be

evaluated, and the current work used characteristic velocity to assess efficiency. The average characteristic velocity C^* could be calculated as

$$C^* = \frac{A_t}{M_t} P_c dt \quad (4)$$

where A_t is the nozzle throat area, and M_t is the mass of the propellant consumed. The average C^* values calculated for all tests are plotted in Figure 8, in which the solid lines indicate the theoretical characteristic velocities, which is calculated using the Chemical Equilibrium with Applications software (Sanford Gordon 1994).

As shown in Figure 10, the combustion efficiencies of the composite grains were lower than that of the PP grain under the same initial experimental conditions, primarily because of the significantly increased regression rates of the former grains. Notably, the characteristic velocity was calculated using P_c instead of $P_{c,s}$ in the present work, which would be expected to provide C^* value lower than the true values. The Al composite grains exhibited the longest startup periods, which also had a significant effect on C^* . Interestingly, the combustion efficiencies of the type B fuel grains were approximately 15.3% and 14.9% greater than those of the type A grains in the case of the ABS and Al grains, respectively. These results are opposite to the effect of perforated structure on the regression rate, that is, the blades with holes provides lower regression rates. One possible explanation is that the holes increased the turbulence within the combustor, thereby improving combustion efficiency, but that this effect was counterbalanced by the enhanced swirl strength of the internal flow, resulting in a decrease in the regression rate. However, this phenomenon is not fully understood at present and more systematic studies, including theoretical work, will be necessary in future.

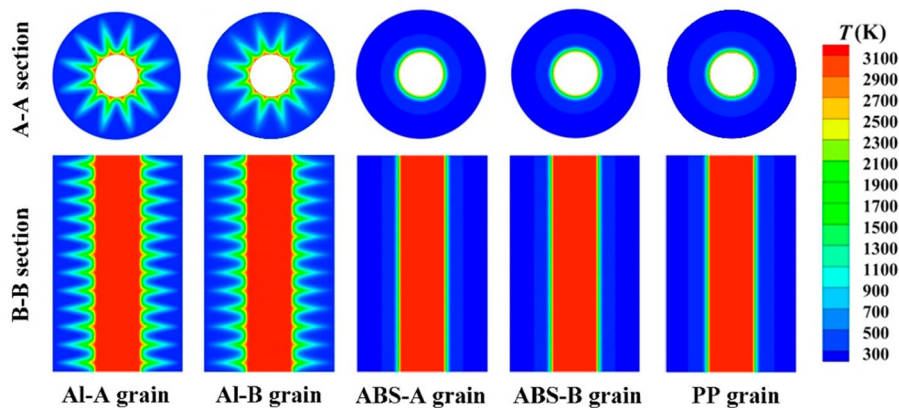


Figure 9. The temperature distributions of the A-A and B-B sections for all fuel grains at 5 s.

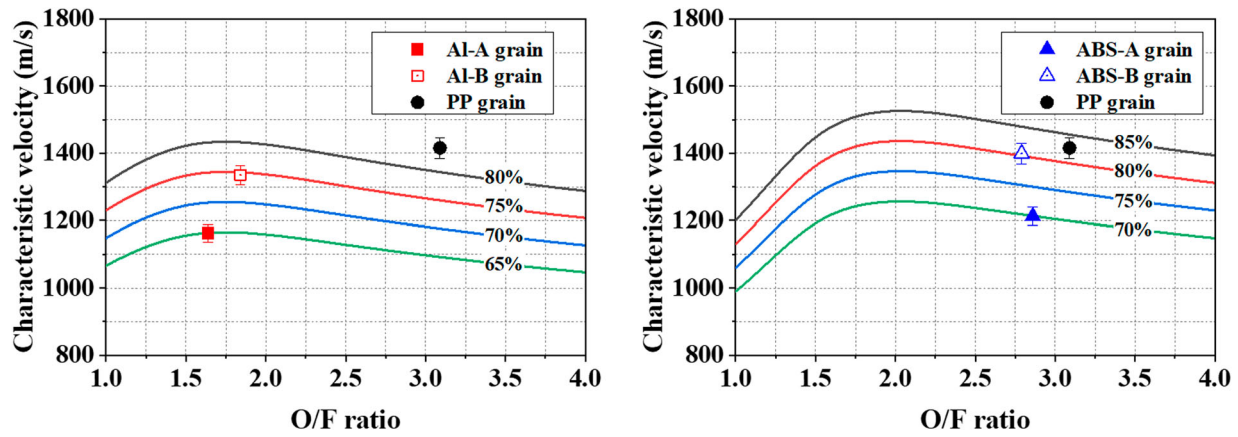


Figure 10. Combustion velocity of each fuel grain as a function of the oxidizer/fuel ratio.

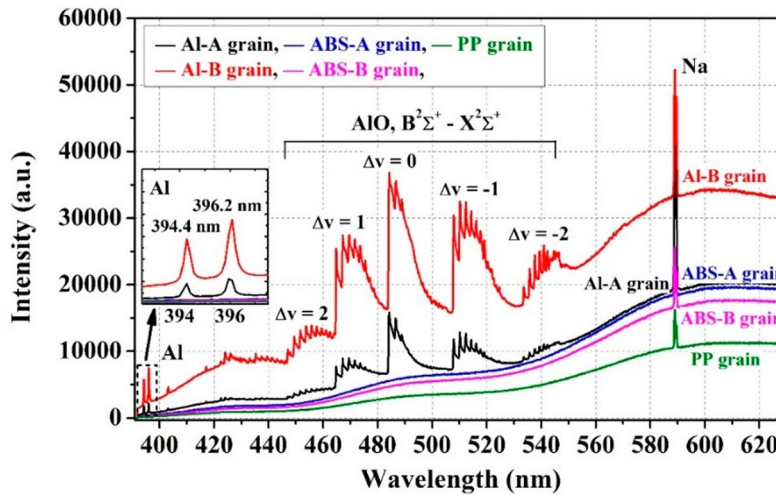


Figure 11. Spectral characteristics of the engine high-temperature plumes obtained from the different fuel grains.

Spectral characteristics of the Al-nested composite fuel grains

Flame spectroscopy is frequently used to identify the atoms and molecules in the combustion zone. The AlO $B^2\Sigma^+-X^2\Sigma^+$ transition is the most prominent feature of Al combustion spectra that has been previously observed in various Al combustion systems (Zhou et al. 2017; Qiu et al. 2021; Goroshin et al. 2007; Knapp et al. 2018). Figure 11 shows the maximum spectral intensities obtained from the five fuel grains during the combustion process. These spectra are interesting in that the AlO $B^2\Sigma^+-X^2\Sigma^+$ transition and Al atomic lines are observed in the data from both the Al-A and Al-B composite fuel grains. AlO radicals in the plume generate a characteristic series of overlapping peaks between 450 and 550 nm. The present study used the AlO $\Delta v = 0$ transition to characterize the overall combustion intensity because this transition had the highest emission intensity. The appearance and disappearance of AlO radicals

could also be used to qualitatively analyze the ignition delay and self-sustaining combustion time of the Al blades.

The intensity of the AlO $\Delta v = 0$ transition was defined as the integrated emission intensity over the wavelength range from 484.11–505.94 nm. The data processing procedure included two steps. First, for each measured emission signal (as shown in Figure 12(a)), a baseline was fitted to the non-radiation wings of the emission feature to subtract the background radiation. The integrated emission intensity was subsequently calculated by taking the integral of the entire emission band from 484.11–505.94 nm, as indicated by the red shading in Figure 12(a). Figure 12(b) presents the AlO $\Delta v = 0$ emission intensities over time for two types of Al composite fuel grains. Note that the time axis here is the same as that used to plot the pressure evolution. It is apparent that AlO radicals appeared sooner during combustion of the Al-B grain, and that these radicals were generated

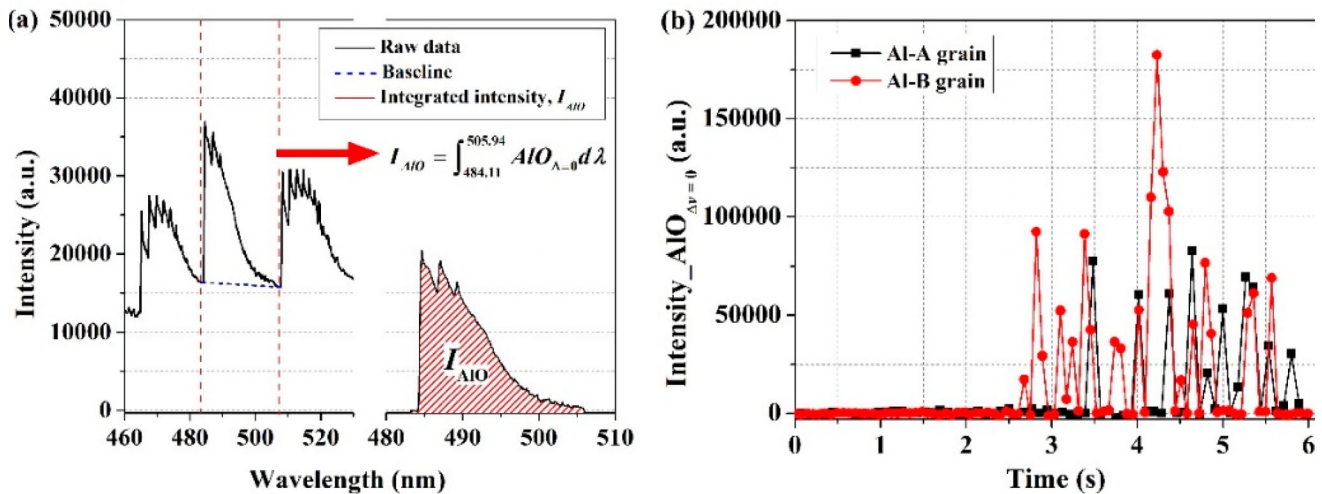


Figure 12. (a) Raw emission spectrum and data processing to determine the emission intensity of the AIO $B^2\Sigma^+-X^2\Sigma^+$ $\Delta v = 0$ transition. (b) The emission intensities of the AIO $\Delta v = 0$ transition during combustion of two types Al composite fuel grains.

more frequently and with greater intensity in the case of the Al-B fuel. The holes in the blades of this specimen are thought to have provided more turbulent combustion and increased the contact area between the spiral blades and the flame, such that it was easier for the Al blades to participate in the combustion reaction. Although it is unclear if the reaction mechanism associated with the present Al blades is similar to that of Al particles (Zhou et al. 2017), these AIO spectra suggest that the Al blades in the composite fuel grains participated in the combustion reaction.

The primary benefits of a nested helical structure (also referred to as a first-level structure) made of metal are significant increases in the mechanical properties and regression rate of the composite grain. However, the present work shows that structural modification of the spiral blades involving a lattice hole structure (the second-level structure) also stiffens the structure and improves the combustion efficiency, albeit at the expense of a slight drop in the regression rate. Future investigations involving either experimental work or numerical simulations are needed to further examine the effects of multi-level metal structures on the mechanical and combustion properties of grains. Quantitative measurement of AIO emissions using multiple lines of sight would also be beneficial.

Conclusion

The mechanical and combustion properties of metal-nested composite hybrid rocket fuel grains were examined, using specimens having an Al framework with twelve spiral blades in which a PP fuel was embedded. ABS composite grains and a PP grain were also tested

for comparison purposes. The mechanical properties of these 3D printed composite grains were studied by means of compression tests and CT technology was employed to investigate meso-damage. The Young's modulus of the Al composite grain was 1194.0% higher than that of the PP grain, while the yield stress of the former specimen was 381.3% higher. The mechanical properties of the Al composite grains were also an order of magnitude greater than those of the ABS composites. The incorporation of lattice holes as a second-level structure on the spiral blades improved the structural stiffness of the grain. The Al substrate bore the majority of stress applied to the grain, resulting in the Al composite grains exhibiting exceptional mechanical properties.

The combustion properties of the Al composite grains were experimentally investigated using lab-scale hybrid rocket engines with gaseous oxygen as the oxidizer at a constant initial mass flow rate of 17.9 g/s. These firing tests assessed ignition characteristics, pressure variations, regression rates and combustion efficiencies. Surprisingly, the regression rate of the Al composite grain was approximately 52.5% higher than that of the PP grain, representing a significant improvement over the enhancement effect of the ABS composite having the same structure (18.0% higher than that of the PP grain). The structural modification of the spiral blades produced other interesting phenomena, such as greatly increased combustion efficiency. An analysis based on non-steady state CFD simulations assessed the effects of the structural and physical properties of the blades on the composite grain combustion performance. This analysis found that the thermal conductivity of the inner blades was the key parameter affecting the regression rate. Finally, a spectral analysis of AIO

radicals in the plumes demonstrated that the Al blades have potential to increase calorific value and density specific impulse of the composite grain.

These results confirm the attractive mechanical and combustion characteristics obtainable from Al composite grains and may have a significant impact on the development of high-performing hybrid rocket fuels. Moreover, the perforated structure demonstrated in this work has shown interesting performance with regard to combustion efficiency, and analyses of different perforated structures should be pursued in future, focusing on flow and combustion effects.

Acknowledgements

The authors thank students Zelin Zhang and Junna Yang from the Institute of Mechanics, Chinese Academy of Sciences for assistance in grain preparation and firing tests and Tibing Wang from the LiM Laser Technology Co. for assisting in fabricating the 3D printed Al frameworks.

Disclosure statement

No potential conflict of interest was reported by the author(s).

Funding

This work was funded in part by the National Natural Science Foundation of China (grant nos. 11802315, 11802309, 12072355, 11872368 and 11927803).

Notes on contributors

Xin Lin is a senior engineer at the Institute of Mechanics, Chinese Academy of Sciences. His research interests include optics and sensors, non-intrusive measurements in harsh environments, hybrid rocket engines and additive manufacturing.

Dandan Qu is an assistant research fellow at the Institute of Mechanics, Chinese Academy of Sciences. Her research interests include extreme environmental materials and structures, metal thermal protection, thermal management, first wall in fusion blanket, laser-matter interaction.

Xuedong Chen is an associate professor at China Agriculture University.

Zezhong Wang is a postdoctoral fellow at the Institute of Mechanics, Chinese Academy of Sciences.

Jiaxiao Luo is a Ph.D. student at the Institute of Mechanics, Chinese Academy of Sciences.

Guoliang Liu is an engineer at the Institute of Mechanics, Chinese Academy of Sciences.

Dongdong Meng is an engineer at the Institute of Mechanics, Chinese Academy of Sciences.

Kun Zhang is an associate professor at the Institute of Mechanics, Chinese Academy of Sciences.

Fei Li is a professor at the Institute of Mechanics, Chinese Academy of Sciences.

Xilong Yu is a professor at the Institute of Mechanics, Chinese Academy of Sciences.

ORCID

Xin Lin  <http://orcid.org/0000-0002-6230-438X>

Dandan Qu  <http://orcid.org/0000-0002-5217-4817>

References

- Akhter, Md. Z., and M. A. Hassan. 2018. "Characterisation of Paraffin-Based Hybrid Rocket Fuels Loaded with Nano-Additives." *Journal of Experimental Nanoscience* 13: S31–S44.
- Arnold, D., J. E. Boyer, K. Kuo, J. K. Fuller, J. Desain, and T. J. Curtiss. 2013. Test of hybrid rocket fuel grains with swirl patterns fabricated using rapid prototyping technology, in: 49th AIAA/ASME/SAE/ASEE Joint Propulsion Conference, AIAA 2013-4141. <https://doi.org/10.2514/6.2013-4141>.
- Arnold, D. M., J. E. Boyer, B. McKnight, K. Kuo, J. Desain, B. B. Brady, J. Fuller, and T. J. Curtiss. 2014. Testing of hybrid rocket fuel grains at elevated temperatures with swirl patterns fabricated using rapid prototyping technology, in: 50th AIAA/ASME/SAE/ASEE Joint Propulsion Conference, AIAA 2014-3754. <https://doi.org/10.2514/6.2014-3754>.
- Bisin, R., C. Paravan, S. Alberti, and L. Galfetti. 2020a. "A new Strategy for the Reinforcement of Paraffin-Based Fuels Based on Cellular Structures: The Armored Grain — Mechanical Characterization." *Acta Astronautica* 176: 494–509.
- Bisin, R., C. Paravan, S. Parolini, and L. Galfetti. 2020b. Impact of 3D-printing on the mechanical reinforcement and the ballistic response of paraffin-based fuels: the armored grain, in: AIAA Propulsion and Energy 2020 Forum, <https://doi.org/10.2514/6.2020-3735>.
- Bouziane, M., A. E. M. Bertoldi, P. Milova, P. Hendrick, and M. Lefebvre. 2019. "Performance Comparison of Oxidizer Injectors in a 1-kN Paraffin-Fueled Hybrid Rocket Motor." *Aerospace Science and Technology* 89: 392–406.
- Broughton, K. M., D. R. Williams, M. J. Brooks, and J. Pitot. 2018. Development of the Phoenix-1B Mk II 35 km apogee hybrid rocket, in: 2018 Joint Propulsion Conference, <https://doi.org/10.2514/6.2018-4838>.
- Cai, G. B., P. Zeng, X. T. Li, H. Tian, and N. J. Yu. 2013. "Scale Effect of Fuel Regression Rate in Hybrid Rocket Motor." *Aerospace Science and Technology* 24: 141–146.
- Cao, Y., X. Lin, Q. Z. Wang, S. Q. Shi, L. Ma, N. Kang, and W. D. Huang. 2021. "Microstructure Evolution and Mechanical Properties at High Temperature of Selective Laser Melted AlSi10Mg." *Journal of Materials Science & Technology* 62: 162–172.
- Casalino, L., and D. Pastrone. 2008. "Optimal Design of Hybrid Rocket Motors for Microgravity Platform." *Journal of Propulsion and Power* 24: 491–498.
- Connell, T., G. Young, K. Beckett, and D. R. Gonzalez. 2019. Enhanced solid fuel regression in a hybrid rocket employing additively manufactured fuels exhibiting novel grain port geometries, AIAA 2019-2015. <https://doi.org/10.2514/6.2019-2015>.

- De Luca, L. T., T. Shimada, V. P. Sinditskii, and M. Calabro. 2017. Chemical rocket propulsion, https://doi.org/10.1007/978-3-319-27748-6_8.
- Fang, S. H., Z. Z. Wang, X. Lin, F. Li, R. J. Li, J. Li, Z. Z. Zhang, Y. Liu, and X. L. Yu. 2021. "Characterizing Combustion of a Hybrid Rocket Using Laser Absorption Spectroscopy." *Experimental Thermal and Fluid Science* 127: 110411.
- Goroshin, S., J. Mamen, A. Higgins, T. Bazyn, N. Glumac, and H. Krier. 2007. "Emission Spectroscopy of Flame Fronts in Aluminum Suspensions." *Proceedings of the Combustion Institute* 31: 2011–2019.
- Hill, C. D., C. C. McDougall, T. L. Messinger, and C. T. Johansen. 2019. Modification of paraffin-based hybrid rocket fuels using structural lattices, in: AIAA Propulsion and Energy 2019 Forum, <https://doi.org/10.2514/6.2019-4191>.
- Hitt, M. A. 2018. Survey of applications of additively manufactured grains in hybrid rocket motors, in: 2018 Joint Propulsion Conference, <https://doi.org/10.2514/6.2018-4712>.
- Jens, E. T., B. J. Cantwell, and G. S. Hubbard. 2016. "Hybrid Rocket Propulsion Systems for Outer Planet Exploration Missions." *Acta Astronautica* 128: 119–130. doi:10.1016/j.actaastro.2016.06.036.
- Joshi, S. C., and A. A. Sheikh. 2015. "3D Printing in Aerospace and its Long-Term Sustainability." *Virtual and Physical Prototyping* 10: 175–185. doi:10.1080/17452759.2015.1111519.
- Kahraman, M., I. Ozkol, and M. A. Karabeyoglu. 2021. "Regression Rate Enhancement of Hybrid Rockets by Introducing Novel Distributed Tube Injector." *Journal of Propulsion and Power*, 1–12. doi:10.2514/1.B38417.
- Karabeyoglu, M. A., and D. Altman. 1999. "Dynamic Modeling of Hybrid Rocket Combustion." *Journal of Propulsion and Power* 15: 562–571.
- Karabeyoglu, M. A., D. Altman, and B. J. Cantwell. 2002. "Combustion of Liquefying Hybrid Propellants: Part 1, General Theory." *Journal of Propulsion and Power* 18: 610–620.
- Knapp, S., S. Kelzenberg, A. Raab, E. Roth, and V. Weiser. 2018. "Emission Spectroscopy of the Combustion Flame of Aluminium/Copper Oxide Thermite." *Propellants, Explosives, Pyrotechnics* 44: 9–17.
- Kobald, M., C. Schmierer, H. K. Ciezki, S. Schlechtriem, E. Toson, and L. T. De Luca. 2017. "Viscosity and Regression Rate of Liquefying Hybrid Rocket Fuels." *Journal of Propulsion and Power* 33: 1245–1251.
- Kuo, K. K., and M. J. Chiverini. 2007. "Fundamentals of Hybrid Rocket Combustion and Propulsion." *American Institute of Aeronautics and Astronautics* 218.
- Marciniak, B., A. Okninski, B. Bartkowiak, M. Pakosz, K. Sobczak, W. Florczuk, D. Kaniewski, et al. 2018. "Development of the ILR-33 "Amber" Sounding Rocket for Microgravity Experimentation." *Aerospace Science and Technology* 73: 19–31.
- Mazzetti, A., L. Merotto, and G. Pinarello. 2016. "Paraffin-based Hybrid Rocket Engines Applications: A Review and a Market Perspective." *Acta Astronautica* 126: 286–297. doi:10.1016/j.actaastro.2016.04.036.
- Ozawa, K., H.-w. Wang, T. Inenaga, and N. Tsuboi. 2020. Accuracy of real-time fuel regression measurement function of a 3D printed solid fuel, in: AIAA Propulsion and Energy 2020 Forum, <https://doi.org/10.2514/6.2020-3741>.
- Oztan, C., and V. Coverstone. 2021. "Utilization of Additive Manufacturing in Hybrid Rocket Technology: A Review." *Acta Astronautica* 180: 130–140.
- Oztan, C., E. Ginzburg, M. Akin, Y. Zhou, R. M. Leblanc, and V. Coverstone. 2021. "3D Printed ABS/Paraffin Hybrid Rocket Fuels with Carbon Dots for Superior Combustion Performance." *Combustion and Flame* 225: 428–434.
- Pabarcus, L. 2019. Development and preliminary testing of paraffin hybrid rocket fuel grains with helical port structures, in: AIAA Propulsion and Energy 2019 Forum, <https://doi.org/10.2514/6.2019-4187>.
- Qiu, Q., Y. N. Zhou, J. Z. Liu, W. Shi, and W. J. Yang. 2021. "Combustion of Aluminum Powder Using CO₂ Laser in O₂/CO₂ Atmosphere Under Different Pressure Conditions." *Journal of Thermal Analysis and Calorimetry*. doi:10.1007/s10973-021-10910-3.
- Sanford Gordon, B. J. M. 1994. Computer program for calculation of complex chemical equilibrium compositions and applications, NASA RP-1311.
- Sella, V., A. Larkey, A. Majumder, A. Rao, Z. Abidi, A. Rando, M. Liu, A. K. Moore, N. Rasmont, and M. F. Lembeck. 2020. Development of a nitrox-paraffin hybrid rocket engine, in: AIAA Propulsion and Energy 2020 Forum, <https://doi.org/10.2514/6.2020-3729>.
- Shinohara, K., and I. Nakagawa. 2012. Regression rate characteristics of paraffin-based fuel under swirled oxidizer flow, in: 48th AIAA/ASME/SAE/ASEE Joint Propulsion Conference & Exhibit, AIAA 2012-4104. <https://doi.org/10.2514/6.2012-4104>.
- Tian, H., Y. L. Li, C. G. Li, and X. L. Sun. 2017. "Regression Rate Characteristics of Hybrid Rocket Motor with Helical Grain." *Aerospace Science and Technology* 68: 90–103. doi:10.1016/j.ast.2017.05.006.
- Uzan, Naor Elad, Roni Shneck, Ori Yeheskel, and Nachum Frage. 2018. "High-temperature Mechanical Properties of AlSi10Mg Specimens Fabricated by Additive Manufacturing Using Selective Laser Melting Technologies (AM- SLM)." *Additive Manufacturing* 24: 257–263.
- Veale, K., S. Adali, J. Pitot, and C. Bemont. 2018. "The Structural Properties of Paraffin wax Based Hybrid Rocket Fuels with Aluminium Particles." *Acta Astronautica* 151: 864–873.
- Wang, Z. Z., X. Lin, F. Li, J. L. Peng, Y. Liu, Z. Z. Zhang, S. H. Fang, and X. L. Yu. 2021a. "Determining the Time-Resolved Mass Flow Rates of Hybrid Rocket Fuels Using Laser Absorption Spectroscopy." *Acta Astronautica* 188: 110–120.
- Wang, Z. Z., X. Lin, F. Li, and X. L. Yu. 2020. "Combustion Performance of a Novel Hybrid Rocket Fuel Grain with a Nested Helical Structure." *Aerospace Science and Technology* 97: 105613.
- Wang, Z. Z., X. Lin, F. Li, Z. L. Zhang, and X. L. Yu. 2021b. "Improving the Combustion Performance of a Hybrid Rocket Engine Using a Novel Fuel Grain with a Nested Helical Structure." *Journal of Visualized Experiments* 167: e61555. doi:10.3791/61555.
- Whitmore, S. A., K. C. Olsen, P. Forster, C. Y. Oztan, and V. L. Coverstone. 2021. Test and evaluation of copper-enhanced, 3-D printed abs hybrid rocket fuels, in: AIAA Propulsion and Energy 2021 Forum, AIAA 2021-3225. <https://doi.org/10.2514/6.2021-3225>.
- Whitmore, S. A., Z. W. Peterson, and S. D. Eilers. 2013. "Comparing Hydroxyl Terminated Polybutadiene and Acrylonitrile Butadiene Styrene as Hybrid Rocket Fuels." *Journal of Propulsion and Power* 29: 582–592.

- Whitmore, S. A., M. Sobbi, and S. Walker. 2014. High regression rate hybrid rocket fuel grains with helical port structures, in: 50th AIAA/ASME/SAE/ASEE Joint Propulsion Conference and Exhibit, <https://doi.org/10.2514/6.2014-3751>.
- Whitmore, S. A., and S. D. Walker. 2017. "Engineering Model for Hybrid Fuel Regression Rate Amplification Using Helical Ports." *Journal of Propulsion and Power* 33: 398–407.
- Whitmore, S. A., S. D. Walker, D. P. Merkley, and M. Sobbi. 2015. "High Regression Rate Hybrid Rocket Fuel Grains with Helical Port Structures." *Journal of Propulsion and Power* 31: 1727–1738.
- Wu, Y., X. L. Yu, X. Lin, S. Li, X. L. Wei, C. Zhu, and L. L. Wu. 2018. "Experimental Investigation of Fuel Composition and mix-Enhancer Effects on the Performance of Paraffin-Based Hybrid Rocket Motors." *Aerospace Science and Technology* 82-83: 620–627.
- Young, G., T. L. Connell, K. Fennell, S. Possehl, and M. Baier. 2021. "Examining Port Geometry/Solid Loading for Additively Manufactured Fuels in Hybrid Rockets." *Journal of Propulsion and Power* 37: 305–313.
- Zdybal, D., L. Pabarcus, A. Laczewski, B. Wyciskiewicz, A. Zwolak, P. Slawcki, and M. Wyzlinski. 2021. Investigation of FDM-printed open-framework-reinforced helical PEWAX grains as a robust, high regression hybrid rocket fuel, in: AIAA Scitech 2021 Forum, <https://doi.org/10.2514/6.2021-1247>.
- Zhang, S., F. Hu, and W. H. Zhang. 2016. "Numerical Investigation on the Regression Rate of Hybrid Rocket Motor with Star Swirl Fuel Grain." *Acta Astronautica* 127: 384–393.
- Zhou, Y., J. Z. Liu, D. L. Liang, W. Shi, W. J. Yang, and J. H. Zhou. 2017. "Effect of Particle Size and Oxygen Content on Ignition and Combustion of Aluminum Particles." *Chinese Journal of Aeronautics* 30: 1835–1843.
- Zilliac, G., G. Story, A. Karp, E. Jens, and G. Wittinghill. 2020. Combustion efficiency in single port hybrid rocket engines, in: AIAA Propulsion and Energy 2020 Forum, <https://doi.org/10.2514/6.2020-3746>.